Constant real-space fractal dimensionality and structure evolution in Ti_{62}Cu_{38} metallic glass under high pressure

Liangliang Li, Luhong Wang, Renfeng Li, Haiyan Zhao, Dongdong Qu, Karena W. Chapman, Peter J. Chupas, and Haozhe Liu

Phys. Rev. B **94**, 184201 — Published 7 November 2016

DOI: 10.1103/PhysRevB.94.184201

Constant real space fractal dimensionality and structure evolution in $Ti_{62}Cu_{38}$ metallic glass under high pressure

Liangliang Li[1, 2], Luhong Wang[1, *], Renfeng Li[1, 2], Haiyan Zhao[3, 4], Dongdong Qu[5], Karena W. Chapman[4], Peter J. Chupas[4], and Haozhe Liu[2, 1, *]

[1]*Harbin Institute of Technology, Harbin 150080, China*

[2]*Center for High Pressure Science and Technology Advanced Research, Changchun 130015, China*

[3]*Center for Advanced Energy Studies, University of Idaho, Idaho Falls, Idaho 83406, USA*

[4]*Advanced Photon Source, Argonne National Laboratory, Argonne, Illinois 60439, USA*

[5]*School of Mechanical and Mining Engineering, The University of Queensland, Brisbane, Queensland 4072, Australia*

The structure of binary $Ti_{62}Cu_{38}$ metallic glass was investigated under pressures up to 33.8 GPa using the pair distribution function (PDF) analysis based on the high energy X-ray scattering and reverse Monte Carlo (RMC) simulations. At global scale, its relative volume showed a continuously smooth curve as a function of pressure. The isothermal bulk modulus of $Ti_{62}Cu_{38}$ metallic glass was estimated as B_0 = 132 (3) GPa with B_0' = 5.8 (0.4). At local scale, atomic packing structure under compression conditions, which was extracted from RMC simulations, showed that the topological short-range order was dominated by the deformed icosahedron polyhedra and basically maintained stable. From the relationship between relative volume and changing ratio of the atomic separation distances, the real space fractal dimensionality of this metallic glass was determined as about 2.5 for all of first four peaks, and this experimental result revealed the consistent nature of fractal feature on degree of self-similarity in this sample within the entire experimental pressure range.

The fractal feature has been suggested in glass system for many years. Very recently, links between the structures of metallic glasses and fractal dimensionality under high pressure conditions were discovered.[1, 2, 3] A power law exponent of 2.5 on the relationship between density and the so-called the 'first strong diffraction peak' in reciprocal space was proposed as a universal feature for metallic glasses under compression.[2, 3] Furthermore, the fractal dimensionality of metallic glasses in real space was found to remain as about 2.5 as well, which was calculated from the atomic nearest-neighbor distance in pair distribution function (PDF) in two typical binary metallic glasses of Cu-Zr and Ni-Al systems up to 20 GPa from classical molecular dynamics (MD) simulations.[1] More interestingly, the pressure dependence of cross-over feature on the power law exponent shifting from 2.5 to 3 with increasing atomic separation distance was proposed, which related to that pressure tune the correlation length change based on continuum percolation model.[1] However, no experimental PDF data was reported to exam the real space fractal dimensionality for any metallic glass system so far, and the validity of these fractal features in real space for metallic glass under high pressure conditions need to be checked by measured data in addition to the MD simulations. Based on this motivation, a typical binary metallic glass Ti-Cu system, which has been studied at ambient conditions for many years,[4-6] was selected as model for the study of structure and real space fractal dimensionality under pressure conditions in this paper.

Due to the complexity of experimental and analysis procedure, investigation on atomic level structure in real space for non-periodic systems under high pressure conditions are exceedingly rare. For example, the limited range of Q in previous high pressure X-ray scattering measurement restricted the accuracy of Fourier transforms to real space PDF, therefore the MD

simulations instead of measured PDF was used to study the structure evolution of metallic glass upon compression.[1] The PDF method is able to provide valuable insights into the local atomic structure, and recently became advanced structure analysis technique combined with synchrotron high energy X-ray scattering measurement with high Q range.[7, 8] Since the PDF method provides real space structural information in one dimension, simulations of the total scattering data using modeling techniques, such as reverse Monte Carlo (RMC), are extremely useful for visualizing the three-dimensional atomic arrangement of liquid and amorphous materials.[9, 10] Furthermore, combined density information derived from RMC fitting with measured PDF, fractal dimensionality of the system, if exists, can be determined in real space.

The total X-ray scattering data for metallic glass $Ti_{62}Cu_{38}$ under high pressure at room temperature were collected at the sector 11-ID-B beamline at the Advanced Photon Source, Argonne National Laboratory, using an incident beam with a size of 150 μm×150 μm and a high energy of 86.7 keV. A 2D large amorphous-silicon-based flat-panel detector was used to record the scattering X-ray. A sample with a dimension of 150 μm ×150 μm ×20 μm was located in the sample chamber, which is a T301 stainless steel gasket with a 270 μm diameter hole between the two anvils of the diamond anvil cell. The pressure medium was 1:4 methanol/ethanol, and pressure was measured using ruby fluorescence method.[11]

Raw two dimensional image data were processed using the Fit-2D[12] software with a masking strategy[13] to mask the diamond peaks to obtain one-dimensional scattering data. After subtracting the contributions from the sample environment and background, the structure factor

S(Q) and reduced PDF *G(r)* were extracted using the PDFgetX2 program,[14] which performs a numerical Fourier transformation between *S(Q)* and *G(r)* according to:

$$G(r) = 4\pi r\rho_0(g(r) - 1) = \frac{2}{\pi}\int_0^\infty Q[S(Q) - 1]\sin(Qr)\,dQ \quad (1)$$

where ρ_0 is the average atomic number density and *g(r)* is the pair distribution function.

The RMC method was performed using a cubic box with periodic boundary conditions containing 10000 atoms to fit the X-ray scattering data for the $Ti_{62}Cu_{38}$ metallic glass using RMC++.[15] A random initial configuration with a number density of 0.0656 $Å^{-3}$ was used for the ambient pressure RMC fitting, where the density was based on measured value by the Archimedes method. At high pressure, the number densities were determined by adjusting the simulation box to provide the best match between the RMC and the experimental data.

Changes in the structure factor *S (Q)* and the corresponding PDF for $Ti_{62}Cu_{38}$ metallic glass at various pressure conditions are displayed in Fig. 1. The splitting of the second peak in both *S (Q)* and PDF observed at each measured pressure is the characteristic indicators for conventional amorphous systems.[16, 17] In reciprocal space, the relation between the first peak position Q_1 and the second peak position Q_2, as well as $Q_{2shoulder}$ which is the position of the shoulder of the second peak, was proposed to relate to specific types of short-range order.[18] For example, the perfect icosahedron short-range order characterized by Q_2 / Q_1 is 1.71 and $Q_{2shoulder} / Q_1$ is 2.04,[19] and the short-range order in liquid pure Ti characterized by Q_2 / Q_1 is 1.76 (0.01) and $Q_{2shoulder} / Q_1$ is 1.92 (0.01).[20] Two Gaussian functions are used to fit the second peak, and the results show that the ratio of the peak positions Q_2 / Q_1 remains as about 1.69 (0.01) and $Q_{2shoulder} / Q_1$ as

about 1.95 (0.01), indicating continuing existence of somewhat distorted icosahedral short-range order in this $Ti_{62}Cu_{38}$ metallic glass.[19, 20]

With increasing pressure, the first peak position Q_1 of the structure factor $S(Q)$ in reciprocal space shifts towards higher Q, while the nearest-neighbor distance r_1 in real space shifts to shorter distances. These characteristic peak shifts reflect the fact of the volume shrinkage and the density increase caused by high pressure. In this work, the density information is derived from RMC simulations. The RMC fit quality at various pressures is also presented in Fig. 1, which displays a good match between the fitting and experimental data. The fitting error of the derived density at each pressure point is within 2.7%. The relative volume V/V_0 of the binary metallic glass $Ti_{62}Cu_{38}$ as a function of pressure are presented in Fig. 2. About 15% decline in volume is observed from ambient conditions to 33.8 GPa. Fitting the data by using the third-order Birch-Murnaghan equation of state (EOS), it is shown that the isothermal bulk modulus of $Ti_{62}Cu_{38}$ is B_0 = 132 (3) GPa when B_0' = 5.8 (0.4). Changes in the relative volume as a function of pressure exhibits a continuously smooth curve, indicating no-detectable phase transition exists within the pressure range investigated in this work.

The first peak position Q_1 and the nearest-neighbor distance r_1 as a function of pressure are shown in inset (a) and (b) of Fig. 2, respectively. The changes in the density related to the first strong peak shifts in both reciprocal space and real space was discovered to follow the power law:[1-3]

$$V/V_0 = \left(Q_{10}/Q_{1P}\right)^{D_{fQ}} \quad \text{or} \quad V/V_0 \propto \left(r_{1p}/r_{10}\right)^{D_{fr}}, \qquad (2)$$

where V_0 is the average atomic volume, Q_{10} is the first peak position of structure factor $S(Q)$ and r_{10} is the nearest-neighbor distance under ambient pressure conditions; V, Q_{1p} and r_{1p} are the corresponding values under high pressure conditions; and D_{fQ} and D_{fr} are the power exponent determined by changing ratio of Q_1 and r_1, respectively. According to the exponent fitting of power law in formula (2), D_{fQ1} of 2.50 (0.01) is determined in reciprocal space by using Q_1 value change. In real space, D_{fr1} is determined as 2.52 (0.04) according to nearest neighbor distance r_1 change, as shown in Fig. 3 (a) and (b), respectively. These results are close to the previous reported values of D_{fQ1} = 2.50[1, 2] and D_{fr1} = 2.54 in other metallic glass systems from MD simulations.[1] The non-integer D_{fQ} and D_{fr} reveal these fractal dimensionalities as scale parameters, which reflect the degree of self-similarity in medium range and short range ordering in currently studied metallic glass system, and are well agreed with the previous reports.[1, 2]

From real space PDF curves at various pressure conditions, fractal dimensionalities were determined by normalized positions of the second peak r_2, the third peak r_3, and the fourth peak r_4 as 2.44 (0.05), 2.59 (0.02), and 2.48 (0.02), respectively, as shown in Fig. 3 (b). The roughly consistent fractal dimensionality as about 2.5 is observed, which surprisingly extend far beyond the nearest neighbor range in real space in this metallic glass system. This is different from the result in previous MD simulations, which suggested power law exponent cross-over phenomenon could be common in metallic glass systems.[1] It is well-known the limitation of classical MD simulation which is strongly depend on quality of potential. As pointed out in the supplementary materials in previous report,[1] the embedded-atomic method (EAM) type potentials used in its MD simulations, normally are not tested at high pressure conditions, which may result in errors. Thus the simulated cross-over of power law exponent from about 2.5 to 3 with increasing atomic

separation distance in real space might not be the general feature in metallic glass system, at least it is not the case for this Ti-Cu glass system. Instead, from the current measured PDF data, the real space fractal dimensionality could remain constant as about 2.5 over large pair distribution range up to above 30 GPa conditions. This consistent nature of fractal dimensionality from various PDF peaks in real space reflects the constant degree of self-similarity in various building block domains in this system, which actually is working well in much bigger atomic separation distance range than that in previous MD simulations.[1] This discovery improves the understanding for real space fractal feature in metallic glass, and offers practical way for the challenging density estimation for non-periodic systems under high pressure conditions by using their measured PDF, without the concerning of the cross-over in its power law exponent when pressure is close to 15 - 20 GPa.[1]

For the PDF peaks higher than the fourth one, the relations between V_p/V_0 and r_{ip}/r_{i0} ($i > 4$) become featureless and could not be fitted according to Eq. (2). This might be related to the limitation effect of correlation length and need more measured data to prove its generality in metallic glass systems. The asymptotic behavior of these PDFs at higher r range could be related to the fractal feature, which was proposed by Ma *et al.*.[21] A sinusoidal function was introduced to describe the oscillatory correlation in far end of the PDF curves in real space, following the early fractal model on colloidal system.[22]

$$g(r) = (A/r^{D-D_f})exp(-r/\xi)sin(Q_1 r - \phi) + 1, \qquad (3)$$

where A is amplitude, $D = 3$ is the dimensionality in 3D Euclidean space, ξ is the cutoff length, Q_1 is the position of the first strong diffraction peak in reciprocal space, and ϕ is a phase. In

$Ti_{68}Cu_{32}$ metallic glass system, $D_f = 2.51$ applied in this equation is the average of D_{fi}, where i = 1, 2, 3, 4.

However, this fractal model of asymptotic behavior was challenged by a recent study based on binary alloy liquid cases,[23] in which the asymptotic behavior of their PDFs could also be fitted well by Ornstein-Zernike (OZ) model, which is a pole analysis for binary system.[24, 25] In OZ approach, asymptotic behavior of PDF could be described as

$$g(r) = (2|\mathcal{A}|/r)exp(-r/\varepsilon)sin(Q_1 r - \theta) + 1, \qquad (4)$$

where $\mathcal{A}$ is amplitude, θ is a phase and ε is decay length. As pointed out previously,[23] the only significant difference between Eqs. (3) and (4) is the power exponent of r.

Using Eqs. (3) and (4), 3-set of typical *g(r)* curves under various pressure conditions were selected for the fitting as shown in Fig. 4. It is clear that both equations mathematically fit almost equally well for the high r range from the fourth peak to 29.99 Å, as are indexed by the very closed values on the goodness-of-fit parameters R^2. All the fitting parameters are summarized in Table I. The fitting results present a tradeoff effect, i. e. the bigger D_f is, the smaller cutoff or decay length would be. It is noted that physical models corresponding to two equations are quite different as discussed previously.[23] Therefore, good fitting of both equations suggests that the proposed asymptotic decay fitting[21] is not the practice method to obtain physical reliable parameters for fractal dimensionality. Instead, the method of relative change of individual peak position in real space PDF could provide more stable scale invariant for fractal dimensionality.

It is interesting to compare the fractal feature between $Ti_{68}Cu_{32}$ metallic glass system under high pressure with other available high pressure case, such as metallic system of liquid gallium. The fractal dimensionality in $Ti_{68}Cu_{32}$ metallic glass system is determined as about 2.5 from the first four PDF peaks uniformly. In contrast, in liquid gallium, the power exponent D_f extracted from both third and fourth peaks are smaller than 3, whereas, from both first and second peaks are bigger than 3, estimated from the measured data.[26] The corresponding parameters of fractal dimensionality in liquid Ga depend on PDF peak positions, which demonstrate its unique physical feature and indicates a more complicated feature than metallic glass cases. Further investigations on liquid Ga under pressure is underway and will be reported elsewhere.

Information on the atomic packing characteristics, such as the bond length, atomic coordination number and local atomic environment, can be extracted from the RMC atomic configurations using the Voronoi tessellation technique.[27, 28] The Voronoi polyhedra are indexed by $<n_3, n_4, n_5, n_6 \ldots>$ to specify the polyhedron type and describe the local environment of the associated central atom, where n_i denotes the number of i-edged faces of a Voronoi polyhedron.

The bond length derived from the Voronoi polyhedron provides the information on an interatomic distances shortening trend as the pressure increasing, as shown in Fig. 5. In particular, the bond length ratio between the solute and solvent atoms, referred to as the effective atomic size ratio, controls the coordination number (CN).[29, 30] The effective atomic size ratio in the current studied metallic glass $Ti_{62}Cu_{38}$ is 1.02, and this ratio remains nearly constant with increasing pressure. The stable effective atomic size ratio generally leads to that the dominant CNs within the first nearest neighbor shell, which are dominated by CN = 12, 13 and 14 as

shown in Fig. 6 (a), do not change with increasing pressure. By the same token, the average CN, Ti-centered average CN and Cu-centered average CN in this metallic glass $Ti_{62}Cu_{38}$ are nearly constant at 13.06 (0.04), 12.86 (0.06), and 13.39 (0.07), respectively, in the first nearest neighbor shell. This modeling result is similar to the result of other metallic glass, such as $Pd_{81}Si_{19}$ system upon compression above 30 GPa, where the CN remains unchanged with increasing pressure as well.[31] Additionally, it is also found that the CN determined by effective atomic size ratio causes that Cu-centered average CN is greater than the Ti-centered CN.[30]

The effective atomic size ratio is also correlated with the type of the coordination polyhedra under pressure.[30] The nearly unchanged effective atomic size ratio leads to a fact that the frequencies of the dominant coordination polyhedral types are similar and they only slightly fluctuate with increasing pressure. The frequencies of the dominant Voronoi polyhedra within the first nearest neighbor shell under three representative pressures 1.0 atm, 18.9 GPa and 33.8 GPa conditions are illustrated in Fig. 6 (b). Note that there is a one-to-one correspondence between the Voronoi index and the coordination polyhedron. Voronoi polyhedra with indices < 0, 2, 8, 1 > and < 0, 0, 12, 0 > corresponding to the deformed prism and icosahedron polyhedra, respectively, both contribute to a small fraction in this system. The polyhedra of deformed crystal feature, which are indexed by < 0, 3, 6, 4 >, < 0, 3, 6, 5 >, < 0, 4, 4, 6 > and < 0, 2, 8, 5 >, contribute 18.1 % and 17.0 % to the entire system, at 1.0 atm and 33.8 GPa, respectively. In contrast, at 1.0 atm and 33.8 GPa, the deformed icosahedron polyhedra indexed by < 0, 2, 8, 2 >, < 0, 3, 6, 3 >, < 0, 1, 10, 2 >, < 0, 2, 8, 3 >, < 0, 2, 8, 4 >, < 0, 1, 10, 3 > and < 0, 1, 10, 4 > amount to the large fractions of 30.3 % and 28.5 %, respectively. It clearly indicates that the deformed icosahedron is the main topological short-range order in the $Ti_{62}Cu_{38}$ metallic glass,

which is consistent with the results obtained from the Q_2 / Q_1 and $Q_{2shoulder}$ / Q_1 ratios analyses. At the local scale, the structure of the $Ti_{62}Cu_{38}$ metallic glass is basically stable as a function of pressure.

In summary, $Ti_{62}Cu_{38}$ metallic glass was investigated using *in-situ* synchrotron high energy X-ray scattering combined with the PDF analysis and RMC fitting under high pressure. The relative volume as a function of pressure was determined as a continuously smooth curve. No major changes existed in the effective atomic size ratio, CN and dominant polyhedron type at various pressure conditions, which indicated the absence of pressure-induced polyamorphism. Moreover, the real space fractal dimensionality as index of degree of self-similarity in this system remained constant as about 2.5, revealing its intrinsic fractal nature within large atomic separation distance up to about 10.5 Å in entire pressure region up to 33.8 GPa.

This work was performed at Argonne National Laboratory and use of the Advanced Photon Source was supported by the US Department of Energy, Office of Science, Office of Basic Energy Sciences, under contract No. DE-AC02-06CH11357. This work was partially supported by Natural Science Foundation of China (U1530402, 11374075), Heilongjiang Province Science Fund for Distinguished Young Scholars (JC201005), Heilongjiang Natural Science Foundation (E200948), Longjiang Scholar, the Fundamental Research Funds for the Central Universities (HIT. BRET1.2010002, HIT. IBRSEM.A.201403), HIT-Argonne Overseas Collaborative Base Project, and Chinese Scholarship Council.

· Electronic email: luhong1@hit.edu.cn and haozhe.liu@hpstar.ac.cn

[1] D. Z. Chen, C. Y. Shi, Q. An, Q. Zeng, W. L. Mao, W. A. Goddard, and J. R. Greer, Science **349**, 1306 (2015).

[2] Q. Zeng, Y. Lin, Y. Liu, Z. Zeng, C. Y. Shi, B. Zhang, H. Lou, S. V. Sinogeikin, Y. Kono, C. Kenney-Benson, C. Park, W. Yang, W. Wang, H. Sheng, H-k. Mao, and W. L. Mao, Proc. Natl. Acad. Sci. **113**, 1714 (2016).

[3] Q. Zeng, Y. Kono, Y. Lin, Z. Zeng, J. Wang, S. V. Sinogeikin, C. Park, Y. Meng, W. Yang, H. K. Mao, and W. L. Mao, Phys. Rev. Lett. **112**, 185502 (2014).

[4] K. H. J. Buschow, Acta Metal. **31**, 155 (1983).

[5] K. B. Kim, K. A. Song, X. F. Zhang and S. Yi, Appl. Phys. Lett. **92**, 241915 (2008).

[6] J. J. Pang, M. J. Tan and K. M. Liew, Appl. Phys. A **106**, 597 (2012).

[7] K. A. See, K. W. Chapman, L. Zhu, K. M. Wiaderek, O. J. Borkiewicz, C. J. Barile, P. J. Chupas and A. A. Gewirth, J. Am. Chem. Soc. **138**, 328 (2016).

[8] P. J. Chupas, K. W. Chapman and P. L. Lee, J. Appl. Cryst. **40**, 463 (2007).

[9] R. L. McGreevy and L. Pusztai, Mol. Simul. **1**, 359 (1988).

[10] R. L. McGreevy, J. Phys.: Condens. Matter **13**, R877 (2001).

[11] H. K. Mao, J. Xu and P. M. Bell, J. Geophys. Res. **91**, 4673 (1986).

[12] A. P. Hammersley, J. Appl. Cryst. **49**, 646 (2016).

[13] K. W. Chapman, P. J. Chupas, G. J. Halder, J. A. Hriljac, C. Kurtz, B. K. Greve, C. J. Ruschman and A. P. Wilkinson, J. Appl. Cryst. **43**, 297 (2010).

[14] X. Qiu, J. W. Thompson and S. J. L. Billinge, J. Appl. Cryst. **37**, 678 (2004).

[15] O. Gereben, P. Jóvári, L. Temleitner and L. Pusztai, J. Optoelectron.: Adv. Mater. **9**, 3021 (2007).

[16] H. H. Wendt and F. F. Abraham, Phys. Rev. Lett. **41**, 1244 (1978).

[17] R. S. Liu, D. W. Qi and S. Wang, Phys. Rev. B **45**, 451 (1992).

[18] H. W. Sheng, E. Ma, H. Z. Liu and J. Wen, Appl. Phys. Lett. 88, 171906 (2006).

[19] K. F. Kelton, G. W. Lee, A. K. Gangopadhyay, R. W. Hyers, T. J. Rathz, J. R. Rogers, M. B. Robinson, and D. S. Robinson, Phys. Rev. Lett. **90,** 195504 (2003).

[20] G. W. Lee, A. K. Gangopadhyay, K. F. Kelton, R. W. Hyers, T. J. Rathz, J. R. Rogers, and D. S. Robinson, Phys. Rev. Lett. **93**, 037802 (2004).

[21] D. Ma, A. D. Stoica, and X. L.Wang, Nature Mater. **8**, 30 (2009).

[22] T. Freltoft, J. K. Kjems, and S. K. Sinha, Phys. Rev. B **33**, 269 (1986).

[23] P. Chirawatkul, A. Zeidler, P. S. Salmon, S. Takeda, Y. Kawakita, T. Usuki, and H. E. Fischer, Phys. Rev. B **83**, 014203 (2011).

[24] R. Evans, R. J. F. Leote de Carvalho, J. R. Henderson, and D. C. Hoyle, J. Chem. Phys. **100**, 591 (1994).

[25] R. J. F. Leote de Carvalho and R. Evans, Mol. Phys. **83**, 619 (1994).

[26] O. F. Yagafarov, Y. Katayama, V. V. Brazhkin, A. G. Lyapin, and H. Saitoh, Phys. Rev. B **86**, 174103 (2012).

[27] J. L. Finney, Proc. R. Soc. Lond. A **319**, 479 (1970).

[28] J. L. Finney, Nature **266**, 309 (1977).

[29] H. W. Sheng, W. K. Luo, F. M. Alamgir, J. M. Bai and E. Ma, Nature **439**, 419 (2006).

[30] H. W. Sheng, Y. Q. Cheng, P. L. Lee, S. D. Shastri and E. Ma, Acta Mater. **56**, 6264 (2008).

[31] H. B. Lou, L. H. Xiong, A. S. Ahmad, A. G. Li, K. Yang, K. Glazyrin, H. P. Liermann, H. Franz, X. D. Wang, Q. P. Cao, D. X. Zhang and J. Z. Jiang, Acta Mater. **81,** 420 (2014).

Captions

Fig. 1. (a) Experimental structure factor *S(Q),* and (b) pair distribution function *g(r)* of the $Ti_{62}Cu_{38}$ metallic glass (blue solid line) at various pressure conditions, with the corresponding RMC fits (red open circle).

Fig. 2. Relative volume V/V_0 of the $Ti_{62}Cu_{38}$ metallic glass as a function of pressure derived from the RMC fit. Blue solid line shows the data fitting using the third-order Birch-Murnaghan EOS. Inset (a) Changes in the ratio of the first peak position Q_1 and (b) nearest-neighbor distance r_1 induced by pressure, respectively.

Fig. 3. The relative volume V/V_0 as a function of (a) the ratio of the first and the second peak positions in reciprocal space, and (b) the ratio of peak position r_i in real space, where i = 1, 2, 3 and 4.

Fig. 4. The fitting results of the asymptotic decay at large *r* range for 3-set of typical *g(r)* using fractal and OZ approach, respectively. The thick gray line presents the *g(r)* from experiment. The thin red and blue line show fits of fractal and OZ model, respectively.

Fig. 5. Bond distance as a function of the pressure. The Cu-Cu, Ti-Ti and Ti-Cu bond length are represented by open circles, squares and open stars, respectively.

Fig. 6. (a) CN distributions and (b) fractions of dominant coordination polyhedra in $Ti_{62}Cu_{38}$ metallic glass under selected pressure conditions of 1.0 atm, 18.9 GPa and 33.8 GPa. Similar trends are found at other pressure points. Note that only the polyhedra with a fraction more than 2% are shown.

TABLE I. The parameters obtained by fitting 3 set of selected $g(r)$ to Eq. (3) based on fractal model and Eq. (4) based on OZ model.

		Fractal model				OZ model			
Pressure	Range (Å)	R^2	ξ (Å)	A	ϕ	R^2	ε (Å)	$\mathcal{A}$	θ
1.0 atm	8.39-29.99	0.958	3.47 (8)	4.6 (3)	0.27 (1)	0.958	4.14 (9)	4.6 (3)	0.27 (1)
18.9 GPa	8.09-29.99	0.969	3.25 (6)	5.4 (3)	0.26 (1)	0.969	3.85 (8)	5.3 (3)	0.26 (1)
33.8 GPa	7.99-29.99	0.957	3.06 (7)	6.7 (5)	0.26 (1)	0.958	3.60 (9)	6.6 (5)	0.26 (1)

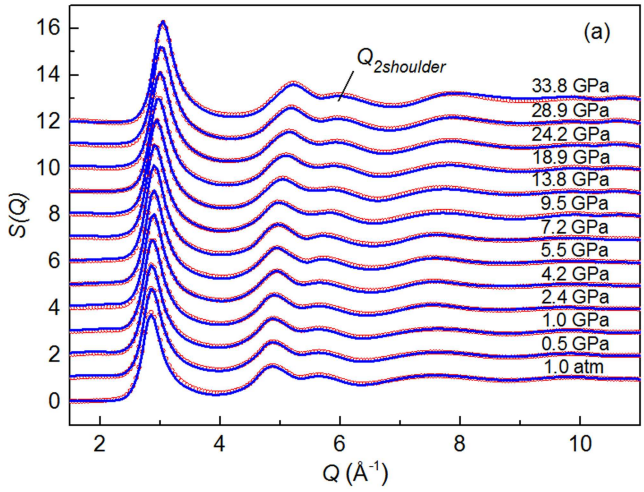

Figure 1a BVR1261B 24OCT2016

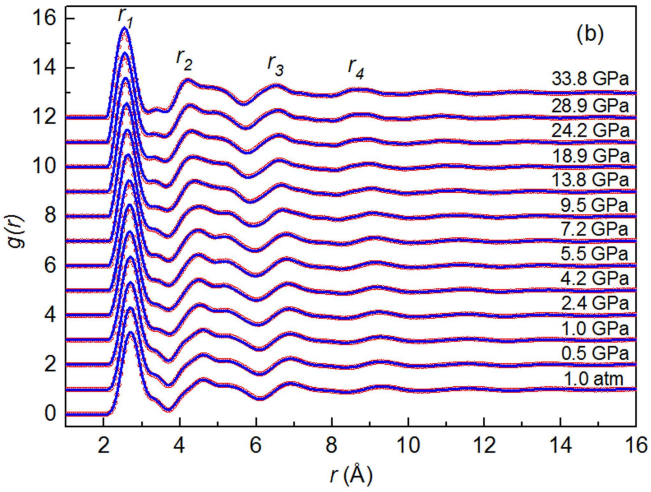

Figure 1b BVR1261B 24OCT2016

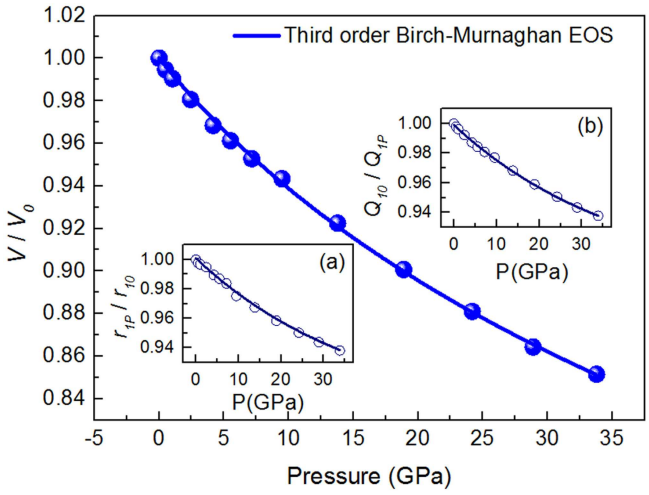

Figure 2 BVR1261B 24OCT2016

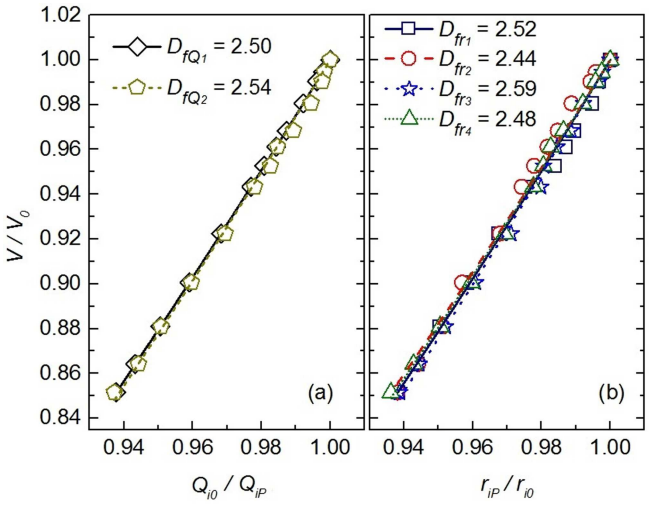

Figure 3 BVR1261B 24OCT2016

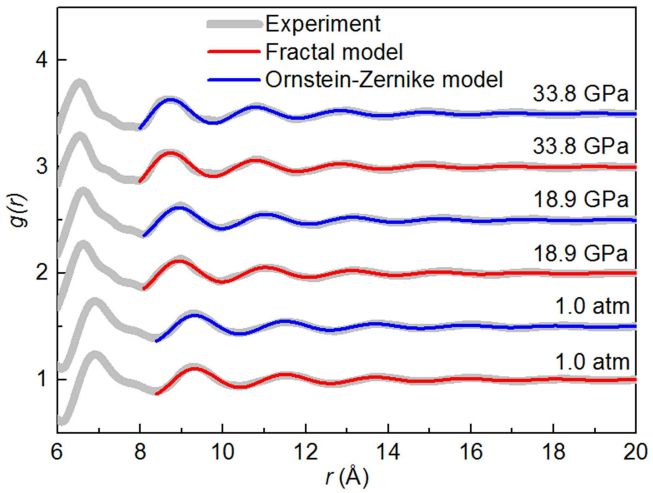

Figure 4 BVR1261B 24OCT2016

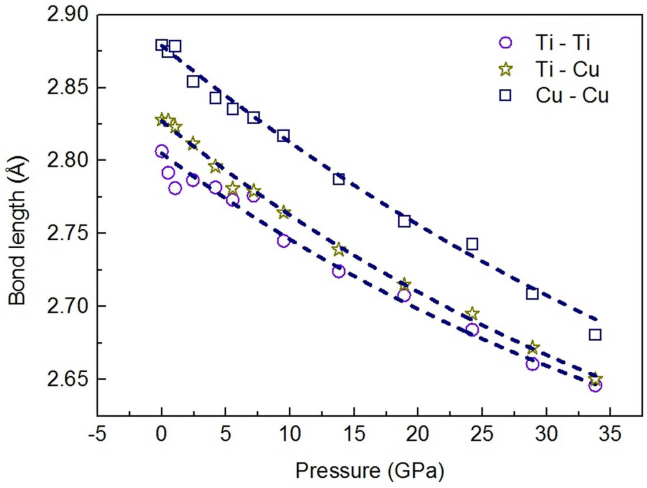

Figure 5 BVR1261B 24OCT2016

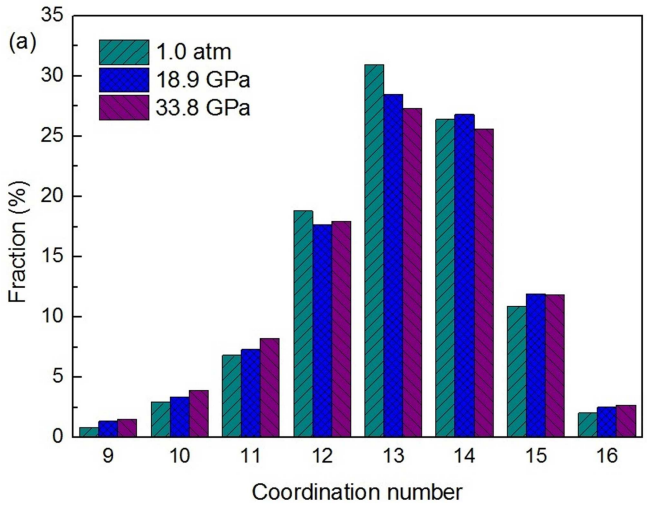

Figure 6a BVR1261B 24OCT2016

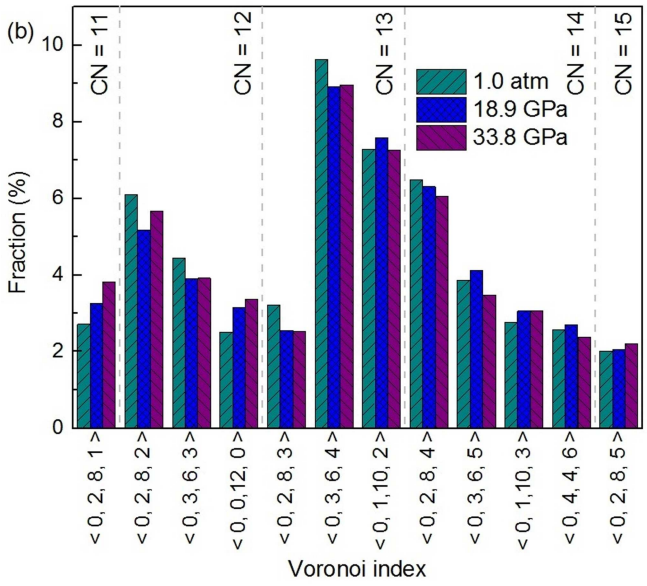

Figure 6b BVR1261B 24OCT2016